A Miniature Manipulator With Variable Stiffness Towards Minimally Invasive Transluminal Endoscopic Surgery

Changsheng Li, *Member, IEEE*, Yusheng Yan, Xiao Xiao, *Member, IEEE*, Xiaoyi Gu, *Student Member, IEEE*, Huxin Gao, Xingguang Duan, *Member, IEEE*, Xiuli Zuo, Yanqing Li, and Hongliang Ren, *Senior Member, IEEE*

***Abstract*—This letter presents a miniature manipulator with variable stiffness towards minimally invasive transluminal endoscopic surgery, such as the endoscopic submucosal dissection (ESD). The manipulator comprises hollow modules with holes in the sidewall, compact with a 4 mm diameter, and dexterous with six degrees of freedom (DOFs). Basic operations of grasping and stripping can be achieved via the terminal surgical tools. The flexible tubes and torque coils are adopted to avoid the motion coupling of the joints. The worm gears with an anti-backdrive property are used to transfer power from the motor to the reels. The variable stiffness is achieved by using the spring-sliding block-based driver system, delivering both high payload/accuracy and flexibility. The system is described in detail. The kinematics, workspace and variable stiffness are analyzed. Tests in terms of the grasping force and variable stiffness are conducted. Results show that the grasping force is larger than 3 N, and the manipulator's stiffness can be tuned with high rates of change. The manipulator's performances, such as the dexterity and the coordination of operation under the master-slave configuration, were preliminarily demonstrated through the basic mock-up operations.**

***Index Terms*—Miniature surgical manipulator, minimally invasive surgery, surgical robotics, transluminal endoscopic surgery, variable stiffness.**

Manuscript received October 15, 2020; accepted February 23, 2021. Date of publication March 23, 2021; date of current version May 25, 2021. This letter was recommended for publication by Associate Editor M. Zecca and Editor P. Valdastri upon evaluation of the reviewers' comments. This work was supported in part by the National Key R&D Program of China under Grant 2018YFB1307700 (including the associated subprogram 2018YFB1307703) from the Ministry of Science and Technology (MOST) of China, in part by the Shun Hing Institute of Advanced Engineering (SHIAE project #BME-p1-21) at the Chinese University of Hong Kong (CUHK), and in part by the National Natural Science Foundation of China under Grants 62073043 and 62003045. *(Corresponding author: Hongliang Ren.)*

Changsheng Li is with the School of Mechatronical Engineering, Beijing Institute of Technology, Beijing 100081, China, with the Beijing Advanced Innovation Center for Intelligent Robots and Systems, Beijing Institute of Technology, Beijing 100081, China, and also with the Department of Biomedical Engineering, National University of Singapore, Singapore 117575, Singapore, and NUS (Suzhou) Research Institute (NUSRI), Suzhou 215123, China (e-mail: lics@bit.edu.cn).

Yusheng Yan is with the Department of Biomedical Engineering, National University of Singapore, 117575, Singapore and also with the College of Mechanical and Electrical Engineering, Harbin Engineering University, Harbin 150001, China (e-mail: yys703@hrbeu.edu.cn).

Xiao Xiao is with the Department of Electrical and Electronic Engineering, Southern University of Science and Technology, Shenzhen 518055, China (e-mail: xiaox@sustech.edu.cn).

Xiaoyi Gu and Huxin Gao are with the Department of Biomedical Engineering, National University of Singapore, Singapore 117575, Singapore, and also with the NUS (Suzhou) Research Institute (NUSRI), Suzhou 215123, China (e-mail: e0019922@u.nus.edu; e0343967@u.nus.edu).

Xingguang Duan is with the School of Mechatronical Engineering, Beijing Institute of Technology, Beijing 100081, China and with the Beijing Advanced Innovation Center for Intelligent Robots and Systems, Beijing Institute of Technology, Beijing 100081, China (e-mail: duanstar@bit.edu.cn).

Xiuli Zuo and Yanqing Li are with the Department of Gastroenterology, Qilu Hospital of Shandong University, Jinan Shandong, China (e-mail: zuoxiuli@sdu.edu.cn; liyanqing@sdu.edu.cn).

Hongliang Ren is with the Department of Electronic Engineering and Shun Hing Institute of Advanced Engineering, The Chinese University of Hong Kong (CUHK), Hong Kong, with the Department of Biomedical Engineering, National University of Singapore, Singapore 117575, Singapore, and also with the NUS (Suzhou) Research Institute (NUSRI), Suzhou 215123, China (e-mail: hlren@ieee.org).

This letter has supplementary downloadable material available at https://doi.org/10.1109/LRA.2021.3068115, provided by the authors.

Digital Object Identifier 10.1109/LRA.2021.3068115

I. Introduction

In RECENT years, minimally invasive surgery (MIS), with the advantages of smaller trauma, less pain, and faster recovery, has been widely used in clinics [1]–[3]. The MIS mainly includes multi-port laparoscopic surgery, single port laparoscopy (SPL), and natural orifice transluminal endoscopic surgery (NOTES). Increasing interests of researchers and surgeons are shifting from multi-port laparoscopic surgery to SPL [4], [5], and NOTES for minimizing the invasiveness of the patients [6]. During the SPL, only a single skin incision with a diameter of 12 mm to 50 mm is required for laparoscopic interventions [7]. The insertion of instruments for NOTES is achieved through a natural orifice without incisions [8]. The diameters of the current surgical robotics for NOTES mainly range from 5 mm to 14 mm [9].

The dexterity of the conventional surgical instruments is insufficient to permit common surgical tasks as the degrees of freedom (DOFs) are constrained by the access port [10], and the collision that may lead to injuries is difficult to be avoided in the confined spaces of the human natural orifice [11]. To address these issues, the robotic-assisted surgical procedure is being developed as a feasible approach and received a great deal of attention [12], [13]. While retaining MIS's features, surgical robotics possess more advantages such as less surgeon's fatigue, higher operation precision, and enabling teleoperation [14]. In view of the fact that most of the operation space for SPL and NOTES is curved, narrow, and surrounded by delicate nerves,

vessels, and sensitive tissue, the surgical robots with flexible and miniature manipulators to achieve dexterous operation are the ideal mechanical design [15]–[17].

Novel surgical robots that possess sufficient dexterity are under continuous development based on the main structures including bar linkages, parallel mechanisms [18]–[20], continuum structures [1], [21] and cable (tendon)-driven systems [7], [22]. Among these structures, continuum structures provide high dexterity with numerous DOFs [23], [24]. However, the effector's weak workload and the difficulties for accurate position control are possible limitations. The cable (tendon)-driven systems can reduce the size of the whole system as the actuators are allowed to be placed far away from the end-effectors [25], [26]. The main concern is that the motion coupling may be caused by the crossed pulling force of the cable (tendon) [27].

Most of the current manipulators are either flexible, increasing the level of safety and maneuverability [28], or rigid, delivering high payload and accuracy, which means these manipulators need to balance these two characteristics at the same time [6]. To address this problem, the manipulator with variable stiffness is taken as an effective solution [29]. As the manipulator's structure should be compact enough, which means it is lack extra space for the structure with variable stiffness, the current technologies for variable stiffness design such as particle jamming technology [30] and thermally activated joints [31] are not applicable.

This letter proposed a miniature manipulator with variable stiffness property, seeking a solution to integrate compact size, flexibility, and dexterity for surgical robotics in MIS. The contributions can be summarized as follows:

- A miniature manipulator is proposed, comprised of the carefully designed hollow modules with holes in the sidewall. It is compact with a diameter of 4 mm and dexterous with six DOFs.The manipulator is driven by wire ropes with flexible tubes. By this driving mode, the joints of the modules are operated separately, avoiding the distractions caused by kinematic coupling. The manipulator's stiffness tune is achieved by the spring-sliding block-based driver system.
- For the manipulator, the kinematics, workspace, and stiffness are analyzed. Tests in terms of the grasping force and variable stiffness are conducted. The manipulator's performance toward the basic operation procedures is demonstrated in the ex vivo test.

The rest of this letter is organized as follows. In Section II, the system, including the manipulator and the driving system, is introduced in detail. Section III presents the workspace and stiffness analysis. Performance tests are introduced in Section IV. The conclusions are summarized in Section VI.

II. System Description

A. System Overview

As shown in Fig. 1, the robotic system consists of a miniature manipulator with variable stiffness (1(a)) and a detachable driver system (1(c)). The close-up view of one wire rope and tube configuration is shown in 1(b). The close-up view of a single driving unit is shown in 1(d). The manipulator and the driver system are connected by flexible tubes.

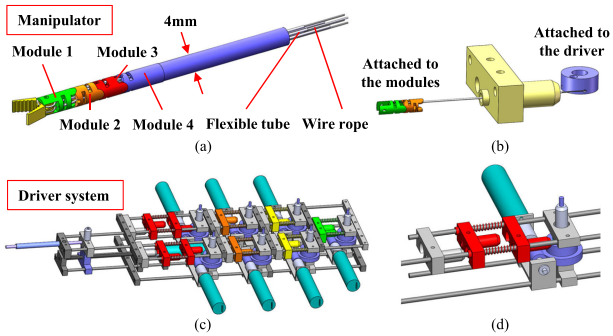

Fig. 1. Robotic system. (a) The manipulator; (b) The close-up view of one wire rope and tube configuration; (c) The driver system; (d) The close-up view of a single driving unit.

B. Manipulator

The manipulator consists of forceps, modules (modules 1 to 4), and wire ropes with flexible tubes. The manipulator's diameter is 4 mm, which is compact enough for dexterous surgical operation. The modules are designed with hollow structures, providing space (inner diameter: 2.8 mm) to allow the wire ropes with flexible tubes to pass through. The arc surface at the ends of the modules is designed for the connection of the adjacent modules. The holes are fabricated by laser cutting (diameter: 0.3 mm) in the modules' sidewall, which provides channels for the wire ropes (diameter: 0.2 mm) to drive the modules. Two wire ropes control each module with flexible tubes (outer diameter: 0.5 mm, inner diameter: 0.3 mm). The joints are driven separately, avoiding the complex motion coupling. The flexible tubes transfer the power from the drive to the manipulator while retaining enough flexibility, ensuring the manipulator can reach the complex and curved human natural orifice. The wire ropes with flexible tubes, used for force transmission allow the driven system to be put far away from the manipulator to ensure the manipulator compact and light enough.

There are six DOFs, including the DOFs for grasping with bending, the DOF for the rotational of the wrist, two DOFs for the manipulator's unfolding, and the translational DOF. The DOF configuration allows the manipulator to move and rotate vertically to the manipulator's axis and move along the axis. The motion states of the manipulator are shown in Fig. 2(a). The manipulator's stiffness is determined by the stiffness of joints 4 and 5.

C. Driver System

As shown in Fig. 2(b), the drive system can be divided into two parts in the consideration that the detachable structure is beneficial to replace the manipulator during the surgery. The reels used to drive the manipulators via wire ropes with flexible tubes are connected to the worm gears by the mechanical interface. The worm gears are driven by direct current (DC) motors (RE13, Maxon motor Inc.). The sliding blocks can move along

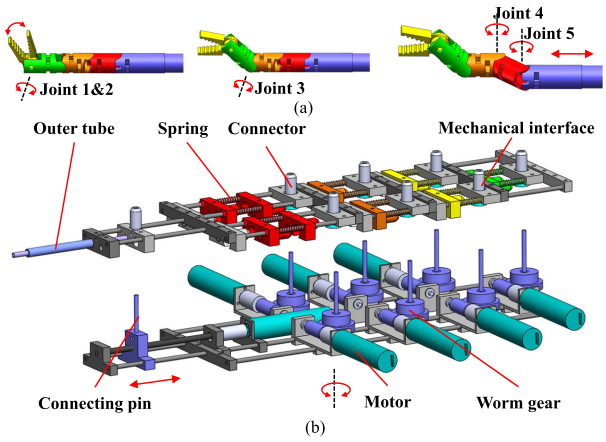

Fig. 2. Details of the robotic system. (a) The manipulator's motion states; (b) Assembling of the driver system.

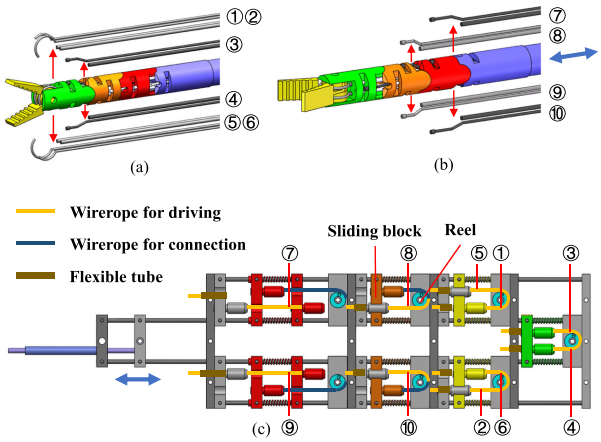

Fig. 3. The connection between the manipulator and the driver system. (a-b) The wire ropes and flexible tubes attached to the manipulator; (c) The wire ropes and flexible tubes attached to the driver system.

the support base rods under the force of the spring and the wire ropes.

The connection between the manipulator and the driver system is illustrated in Fig. 3. As shown in Fig. 3(a) and (c), the wire ropes with flexible tubes ① and ⑤ are attached to one forceps (wire ropes) and the module 1 (flexible tubes). The wirerope with flexible tubes ② and ⑥ are attached to the other forcep and module 1. The motion of rotation and grasping are controlled by the reels in the driver system via these wire ropes. The springs are applied to the flexible tubes ① and ⑥ as a serial elastic actuation (SEA) for better performance. The stiffness of the SEA can be tuned via the spring. The SEA is not applied to the flexible tubes ② and ⑤, aiming to provide enough grasping force. Wire ropes with flexible tubes ③ and ④ are attached to module 1 (wire ropes) and module 2 (flexible tubes). The wrist's bending is driven by the reels via these wire ropes with the springs applied as SEA.

Fig. 3(b) and (c), wire ropes with flexible tubes ⑦ and ⑨ are attached to module 3(wire rope)/module 4 (tube), and module 2 (wire rope)/module 3 (tube), respectively, providing adjustable

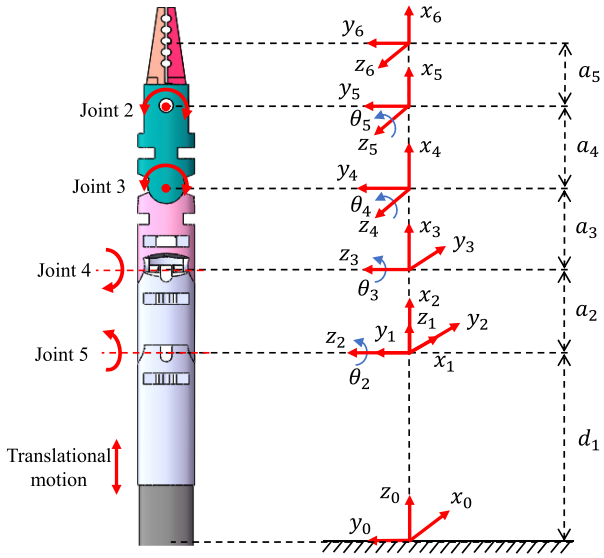

Fig. 4. Kinematics analysis of the manipulator.

force to control the manipulator's stiffness by the corresponding spring. If the spring's compression keeps constant, which is controlled by the rotation of the reel, the manipulator's stiffness is not affected by the manipulator's motion. In this case, the rotation of the reel is calculated according to the manipulator's pose via inverse kinematics. Wire ropes with flexible tubes ⑧ and ⑩ are also attached to module 3(wire rope)/module 4 (tube), and module 2 (wire rope)/module 3 (tube), respectively, providing adjustable length to control the manipulator's pose. The wire rope attached to the reels and the sliding block is used to fix the reels in the initial state.

The haptic device (Geomagic Touch Haptic Device, Sensable Technologies Inc.) with 6 DOFs is used to control the manipulator's motion, allowing the teleoperation under the master-slave configuration. The personal computer (PC) running Matlab/Simulink programs works as the controller. The input signals of the programs are from the haptic device. The mapping between the pose of the haptic device and the manipulator is established via the manipulator's kinematics. The programs' output signals control the motor's motion via the driver (RMDS-108, RoboModule Inc.).

III. Analysis

A. Kinematics

The manipulator's kinematics is established and analyzed in this section. As shown in Fig. 4, $x_0y_0z_0$ is defined as the base coordinate system established on the manipulator's fixed support. $x_1y_1z_1$ representing the manipulator's overall movement along the axis is established at the rotation joint 5. $x_2y_2z_2$, $x_3y_3z_3$, $x_4y_4z_4$, and $x_5y_5z_5$ are correspondingly located at the rotation joints 5, 4, 3, and 2 according to the right-hand rule. The origin of $x_1y_1z_1$ coincides with that of $x_2y_2z_2$. Furthermore, $x_6y_6z_6$ represents the tool coordinate system, reflecting the forceps'

TABLE I
DH PARAMETERS FOR THE KINEMATICS

Joint i	α_{i-1}	a_{i-1}	a_{i-1}	θ_i
1	0	0	d_1	0
2	$-\pi/2$	0	0	$-\pi/2+\theta_2$
3	0	a_2	0	θ_3
4	$\pi/2$	a_3	0	θ_4
5	0	a_4	0	θ_5
6	0	a_5	0	0

position and pose. The Denavit-Hartenberg(DH)'s parameters are given in Table I.

The coordinate transformation matrix between adjacent joints i and i-1 can be expressed by

$$T_i^{i-1}=\begin{bmatrix} c\theta_i & -s\theta_i & 0 & a_{i-1} \\ s\theta_i c\alpha_{i-1} & c\theta_i c\alpha_{i-1} & -s\alpha_{i-1} & -s\alpha_{i-1}d_i \\ s\theta_i s\alpha_{i-1} & c\theta_i s\alpha_{i-1} & c\alpha_{i-1} & c\alpha_{i-1}d_i \\ 0 & 0 & 0 & 1 \end{bmatrix} \tag{1}$$

where c and s represent the functions cosine and sine, respectively.

By introducing the kinematic parameters in Table I into the formula (1), all homogeneous transformation matrices T_1^0, T_2^1, T_3^2, T_4^3, T_5^4, and T_6^5 are obtained in turn. And then, the forward kinematics of the manipulator can be deduced as follows:

$$T_6^0=T_1^0\cdot T_2^1\cdot T_3^2\cdot T_4^3\cdot T_5^4\cdot T_6^5=\begin{bmatrix} \boldsymbol{n} & \boldsymbol{o} & \boldsymbol{a} & \boldsymbol{p}_6^0 \\ 0 & 0 & 0 & 1 \end{bmatrix} \tag{2}$$

where $\boldsymbol{p}_6^0=[p_x \quad p_y \quad p_z]$ represents the position matrix of the end forceps in the base coordinate system, and $\boldsymbol{R}_6^0=[\boldsymbol{n} \quad \boldsymbol{o} \quad \boldsymbol{a}]$ represents the pose matrix of 3×3.

Considering that the parameter a_5 is determined by the manipulator's mechanical structures, the transformation matrix T_6^5 is a constant matrix. To solve the inverse kinematics, the pose information of the end forceps in the base coordinate system is given as the formula (3) in the command.

$$T_6^0=\begin{bmatrix} n_x & o_x & a_x & p_x \\ n_y & o_y & a_y & p_y \\ n_z & o_z & a_z & p_z \\ 0 & 0 & 0 & 1 \end{bmatrix} \tag{3}$$

Left multiplying both sides of the formula (3) simultaneously by the inverse matrix of T_0^1, the following expression can be obtained.

$$(T_1^0)^{-1}\cdot T_6^0=T_2^1\cdot T_3^2\cdot T_4^3\cdot T_5^4\cdot T_6^5 \tag{4}$$

By combining (3) and (4) and using the equality of the corresponding elements on the left and right matrices, the overall manipulator's rotation variable can be first solved as follows:

$$\begin{aligned} d_1 &= p_z + a_3a_x + a_5o_ya_x \\ &\quad + a_4a_x\sqrt{1-((p_y-a_5n_y)/a_4)^2} - a_2\sqrt{1-M^2} \end{aligned} \tag{5}$$

where

$$M=(p_x-a_3a_z-a_5o_ya_z - a_4a_z\sqrt{1-((p_y-a_5n_y)/a_4)^2})/a_2 \tag{6}$$

Meanwhile, the rotational variables corresponding to the joints 4 and 2 can also be solved as:

$$\begin{aligned} \theta_2 &= \operatorname{asin}((p_x-a_3a_z-a_5o_ya_z \\ &\quad - a_4a_z\sqrt{1-((p_y-a_5n_y)/a_4)^2})/a_2) \end{aligned} \tag{7}$$

$$\theta_4=\operatorname{asin}((p_y-a_5n_y)/a_4) \tag{8}$$

Similarly, by several transformations of (4), the inverse kinematics solution of other controlled joints can be obtained as follows:

$$\theta_3=\operatorname{asin}(a_z\sqrt{1-M^2}+a_xM) \tag{9}$$

$$\begin{aligned} \theta_5 &= \operatorname{asin}(n_y\sqrt{1-((p_y-a_5n_y)/a_4)^2} \\ &\quad + (n_za_x-n_xa_z)(p_y-a_5n_y)/a_4) \end{aligned} \tag{10}$$

It should be specially mentioned that in the process of solving inverse kinematics, the controllable range of each rotation joint is constrained as follows according to the design:

$$\begin{cases} d_1\in[41,61] \\ \theta_2\in[0,\pi/4] \\ \theta_3\in[-\pi/4,0] \\ \theta_4\in[-\pi/4,\pi/4] \\ \theta_5\in[-\pi/2,\pi/2] \end{cases} \tag{11}$$

The above analysis demonstrates that inverse kinematics' unique analytical solution can be obtained for the designed surgical manipulator within the range of motion, providing a theoretical basis for motion control.

B. Workspace Characterization

The workspace of the proposed robotic system is evaluated through experiments and simulation. As shown in Fig. 5, The manipulator was driven to its limit positions. The opening angle of the forceps achieved by joint 1 and 2 was 60°(Fig. 5(a)). The rotational angle of the wrist joint 3 was 45°(Fig. 5(b)). The radial translation of the wrist was 5 mm (Fig. 5(c)). The inward bending angle achieved by joint 4 and the outward bending angle achieved by joint 5 were both 30°(Fig. 5(d–e)). The radial translation achieved by the joint 4 and 5 was 5 mm (Fig. 5(f)).

The simulated workspace based on the kinematics via Matlab software is shown in Fig. 6. Results show that it covers an area of 25 mm × 16 mm × 20 mm. The experiment and the simulation demonstrate the robotic system's ability to reach the surgical target region, providing a reference for the MIS application.

C. Variable Stiffness Analysis

Figure 7 shows the schematic representation of the force tuning for variable stiffness. The sliding blocks with the spring can move along the rod. One of the sliding blocks is attached to the wire rope, and the other is attached to the worm gear via the extra wire rope. The initial length of the spring is l_0. If the stiffness is tuned, the length of the spring is l'. The pull force

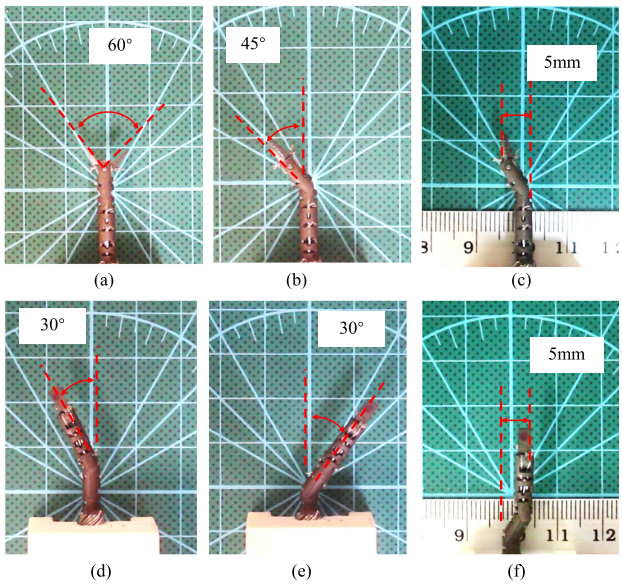

Fig. 5. Workspace demonstration of the robotic system. (a) The opening angle of the forceps achieved by joint 1 and 2; (b) The rotational angle of the wrist joint 3; (c) The radial translation of the wrist; (d) The inward bending angle achieved by the joint 4; (e) The outward bending angle achieved by the joint 5; (f) The radial translation achieved by the joint 4 and 5.

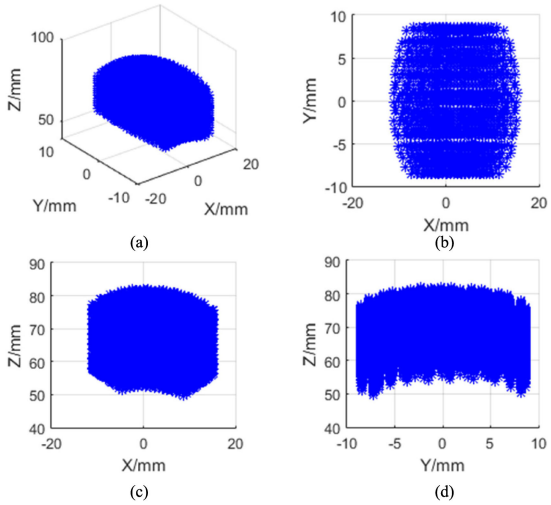

Fig. 6. Simulated workspace based on the kinematics via Matlab software: (a) Side view; (b)$x-y$ plane view; (c) $x-z$ plane view; (d) $y-z$ plane view.

F_S of the wire rope can be described by

$$F_S = k(l_0 - l') \tag{13}$$

where k is the elastic coefficient of the spring. This equation provides a reference for the manipulator's stiffness tuning. As wire rope 1 is driven by force control and wire rope 2 is driven by position control, the manipulator's stiffness is determined by wire rope 2. The pulling force F_S is related to l' and k, which means that the manipulator's stiffness is increased if l' is decreased or k is increased. l' is determined by the rotation of the worm gears, which means the stiffness of the joint can be tuned in real-time.

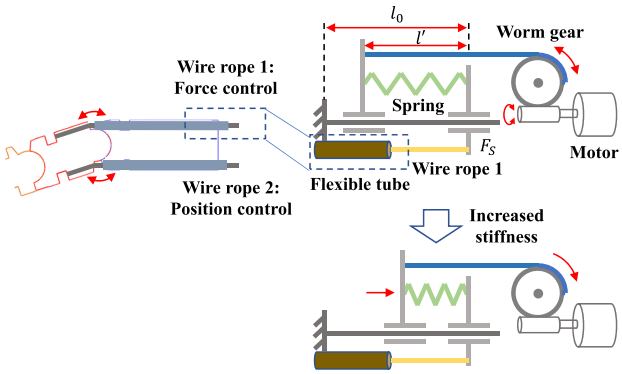

Fig. 7. Schematic representation of the force tuning for variable stiffness.

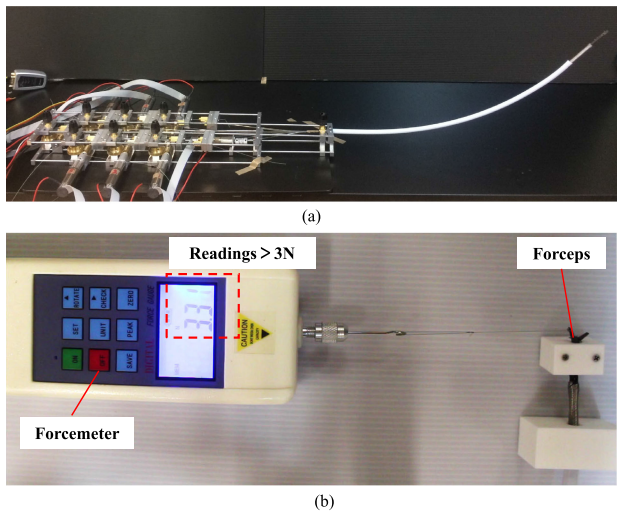

Fig. 8. Test for grasping force. (a) prototype of the manipulator with the driver system; (b) The experimental setup and the results.

IV. Experimental Verification

A. Test for the Grasping Force

In this section, we evaluate the grasping force of the forceps by a simple test. As the forceps is compact, it is difficult to test the grasping force directly. Hence we tested the force of one forcep as the grasping force. The prototype of the manipulator with the driver system is shown in Fig. 8(a). In Fig. 8(b), the manipulator was fixed to the support, and the manipulator's side fixed the force meter in a vertical direction. The terminal of the force meter was attached to the forceps via a wire rope. In the test, the forcep was driven to rotate with the tension readings displayed on the force meters screen from 0 to 3.31 N. It means that the grasping force achieved by the forceps is larger than 3 N, which is satisfied with most regular operations such as knotting, suturing, and holding the surgical instruments [32].

B. Test for the Variable Stiffness

The manipulator's stiffness in two conditions is tested and evaluated in this section. As shown in Fig. 9, the manipulator was fixed on the support. A force sensor (Resolution: 2.5 mN,

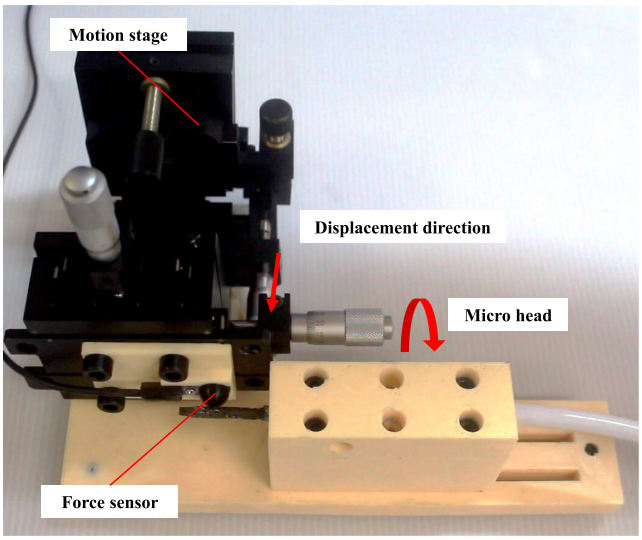

Fig. 9. Experimental setup of the variable stiffness test.

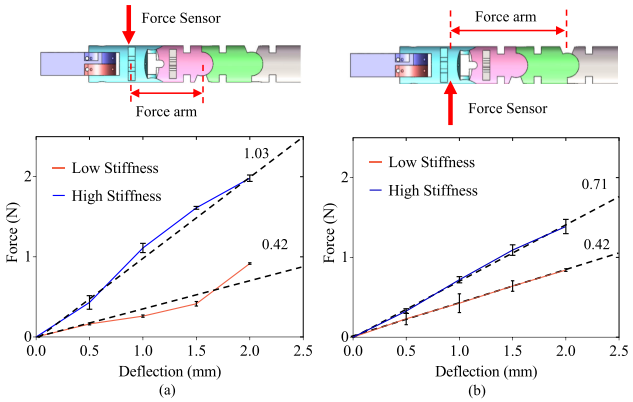

Fig. 10. Results of the variable stiffness test. (a) The relationship between force and deflection on direction I; (b) The relationship between force and deflection on direction II.

OMD-10-SE-10 N, Optoforce Ltd.) was mounted to the motion stage, with its top kept in touch with the side of the manipulator. As the manipulator's structure is asymmetric, both directions' stiffness was tested, vertical to the rotation axes for deployment. In each direction, two states, including low stiffness and high stiffness, were set. The micro head on the motion stage was rotated to drive the force sensor to move from 0 to 2 mm with a step of 0.5 mm, repeating 5 times. The manipulator followed the movement of the force sensor. The reaction force reading from the force sensor and the displacement of the force sensor that reflected the manipulator's deflection was recorded. The manipulator's stiffness can be obtained via these two parameters.

The results of the test are shown in Fig. 10. The manipulator's stiffness is described by the ratio between the force and the deflection. The ratio increases evenly with the deflection and can be fitted as a straight line. For the direction I, the stiffness of the two states is 0.42 N/mm and 1.03 N/mm, with a change rate of 2.45. For the direction II, the stiffness of the two states is 0.42 N/mm and 0.71 N/mm, with a change rate of 1.69. The

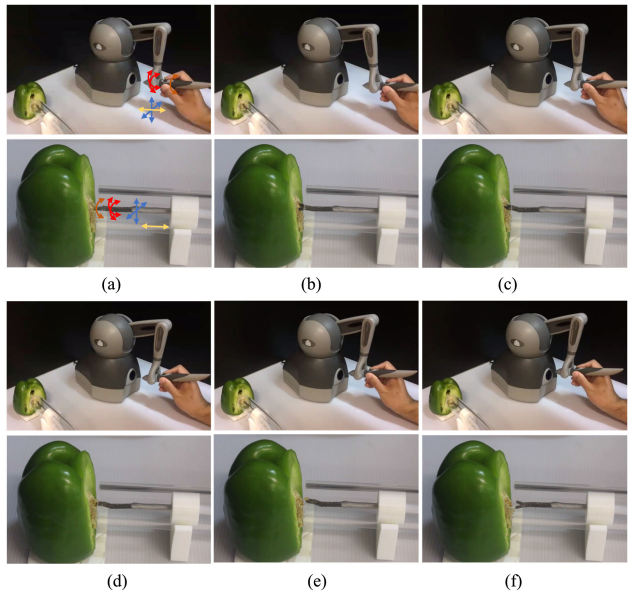

Fig. 11. Performance of picking up green pepper seeds. (a) The manipulator's initial state; (b) The manipulator was reaching to the target region; (c-d) The process of picking the seeds; (e) The manipulator was retrieve from the target region; (f) The seeds was dropped.

degree of the change rate is obvious in both directions. The distinction is that the change rate on the direction I is larger than that on direction II, caused by the different length of the force arm for tuning the stiffness. This experiment is conducted to verify whether the mechanism for tuning the stiffness is effective. According to the surgeries' requirements, the manipulator's stiffness is customized by modulating the elastic coefficient of the springs.

C. *Performance Test*

This experiment is conducted to pick up and drop the green pepper seeds. A haptic device is used on the master side. To simplify the mapping, the three-translation DOFs and the two-rotation DOFs of the manipulator's terminal are corresponding with that of the haptic device. The grasping DOF is corresponding with the rotation DOF of the haptic device. The operation process is shown in Fig. 11. The manipulator was placed in a transparent tube with a diameter of 20 mm that simulated the human's natural cavity. The green chilli with seeds was put in front of the manipulator, which represented the operation objects (Fig. 11(a)). After the initial setup, the manipulator was controlled to reach the target region in the green chilli by the operator via the master device (Fig. 11(b)). The forceps were steered to open (more than 60°) and picked up the seeds (Fig. 11(c–d)). After that, the manipulator was retrieved from the target region (Fig. 11(e)), and dropped the seeds on the table to finish the operation (Fig. 11(f)). The whole process from picking up to drop the seeds lasted 10 s. The manipulator's performance, such as the manipulator's dexterity and the coordination under the master-slave configuration, was preliminarily demonstrated through these basic operations.

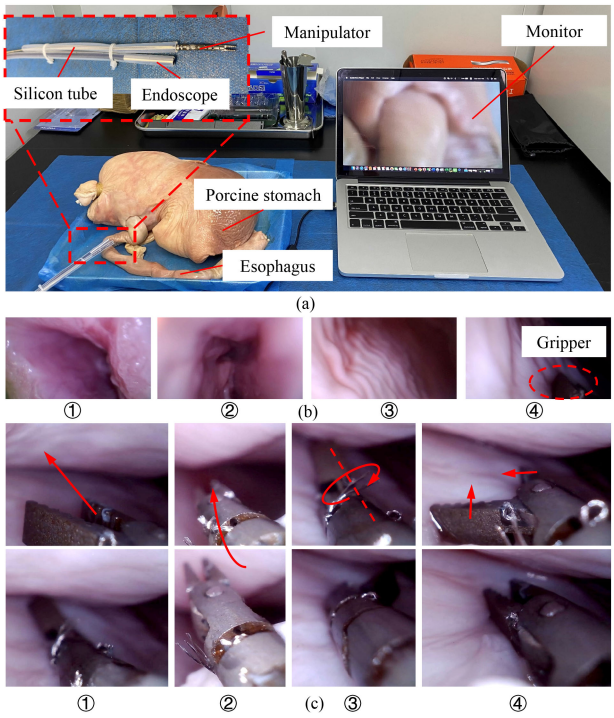

Fig. 12. Ex vivo test. (a) Experimental setup; (b) Operation process: ① esophagus entrance, ② inner esophagus, ③ stomach wall, ④ target region; (c) Movement tests: ① translation, ② bending, ③ rotation, ④ gripper closing. The upper row displays the manipulator's initial position while the lower row shows the ending position.

D. Ex Vivo Test

The experimental setup is presented in Fig. 12(a), including the manipulator, an endoscope (diameter: 3.9 mm, focus length: 10 mm, resolution: 1280*720), a porcine stomach with the esophagus, and a monitor. In real operation, the manipulator needs to pass through the corresponding channel of the endoscope and is controlled in the fashion of teleoperation. However, in our case, we use two silicone tubes (diameter: 4 mm) to simulate two channels of a real endoscope platform. The endoscope and manipulator are inserted into two silicone tubes and are bound together. The endoscope is connected to the PC monitor by a USB cable. Preoperatively, the porcine stomach is inflated manually.

The operation procedures are shown in Fig. 12(b). The endoscope was wrapped inside the silicon tube before entering the stomach. The simulated endoscope platform was steered to pass from esophagus entrance (Fig. 12(b)-①) to stomach wall (Fig. 12(b)-③). After reaching the target region (Fig. 12(b)-④), the platform was fixed, and then the manipulator was pushed out successfully to carry out the following tests. In the last step, the manipulator may be blocked by some tissues on the stomach wall, such as the polyps and mucous membrane, caused by a sharp corner of the gripers.

Inside the porcine stomach, four-movement tests were conducted, as shown in Fig. 12(c), including translation, bending, rotation (entire model), and gripper closing. The manipulator finished the translation smoothly, as shown in Fig. 12(c)-①, which means that the friction between the transmission tube of the manipulator and the internal wall of the endoscope channel is small. Nevertheless, the bending movement(Fig. 12(c)-②) was restricted by the stomach wall. However, the manipulator has enough force to overcome the resistance. Additionally, to prove the manipulator can move flexibly inside the channel, we rotate the driver part to make the manipulator revolute about its central axis. The Fig. 12(c)-③ presents the successful rotation, which means that enough torque can be transmitted to the manipulator despite the long length of the transmission part of the manipulator and friction with the tissue surface. Finally, the gripper can open and close successfully in the narrow space, as shown in Fig. 12(c)-④. All of the tests show that the designed manipulator has as high flexibility inside the porcine stomach as outside, which is also helpful for the future in vivo test.

The real stomach environment is significantly complicated, such as narrow space, soft tissues and mucous membrane. In practice, the manipulator's dexterity is prone to be affected by the narrow space of organs, and the grippers sometimes are difficult to grasp the target due to the mucus and deformation of the stomach. Therefore, these tests are carried out to validate the manipulator's dexterity and the grasping capability of the grippers in actual operation. Additionally, the correct operating procedures of this NOTES system are important for the designed manipulator to work normally inside the stomach. Hence, the other purpose of these tests is to simulate the real operation procedures.

V. Conclusions

This letter presents a miniature manipulator with variable stiffness towards minimally invasive surgery (MIS). The manipulator is composed of hollow modules with holes in the sidewall, compact with a diameter of 4 mm, and dexterous with six DOFs. The wire ropes with flexible tubes are adopted to avoid the motion coupling of the joints. This design differs from most of the current cable (tendon)-driven systems without tubes for force transmission in the manipulator [33], [34]. The driver system is designed to be divided into two parts to change the manipulator during the surgery. The worm gears with an anti-backdrive property are used to transfer power from the motor to the reels. The manipulator's variable stiffness is achieved by using the spring-sliding block-based driver system.

The system, including the manipulator and the driver system, is described in detail. The kinematics is analyzed as the basis of the motion control. Through experiments, the workspace is evaluated, showing the forceps' open-angle, bending angle, and the manipulator's translation. Besides, the principle of manipulator's variable stiffness is analyzed. Tests in terms of the grasping force, variable stiffness are conducted. Results show that the grasping force is larger than 3 N, which is satisfied with most of the regular operation, and the manipulator's stiffness can be tuned with a change rate of 2.45 and 1.69. The manipulator's performances, such as the manipulator's dexterity and the coordination of operation under the master-slave configuration, were preliminary demonstrated through the basic operation. As the application, the manipulator is equipped as a device operated in the NOTES environment. The ex vivo test is conducted to demonstrate the surgical procedures.

In this robotic system, only one manipulator is developed for proof-of-concept, and most of the complex operations in MIS require multiple arms. In the future, we will propose multi-manipulators to achieve collaborative operation. More operations will be conducted for the ex vivo test, including grasping, cutting under the teleoperated configuration.

REFERENCES

[1] J. Burgner-Kahrs, D. C. Rucker, and H. Choset, "Continuum robots for medical applications: A survey," *IEEE Trans. Robot.*, vol. 31, no. 6, pp. 1261–1280, Dec. 2015.

[2] C. Li, N. K. K. King, and H. Ren, "A skull-mounted robot with a compact and lightweight parallel mechanism for positioning in minimally invasive neurosurgery," *Ann. Biomed. Eng.*, vol. 46, no. 10, pp. 1465–1478, Oct. 2018.

[3] X. Xiao, H. Gao, C. Li, L. Qiu, and H. Ren, "Portable body-attached positioning mechanism toward robotic needle intervention," *IEEE/ASME Trans. on Mechatronics*, vol. 25, no. 2, pp. 1105–1116, Apr. 2020.

[4] M. Piccigallo *et al.*, "Design of a novel bimanual robotic system for single-port laparoscopy," *IEEE/ASME Trans. Mechatronics*, vol. 15, no. 6, pp. 871–878, Dec. 2010.

[5] K. Yung, J. Cheung, S. Chung, S. Singh, and C. Yeung, "A single-port robotic platform for laparoscopic surgery with a large central channel for additional instrument," *Ann. Biomed. Eng.: J. Biomed. Engineering Soc.*, vol. 45, no. 9, pp. 2211–2221, 2017.

[6] Y. Li *et al.*, "Super: A surgical perception framework for endoscopic tissue manipulation with surgical robotics," *IEEE Robot. Automat. Lett.*, vol. 5, no. 2, pp. 2294–2301, Apr. 2020.

[7] H. Choi, H. Kwak, Y. Lim, and H. Kim, "Surgical robot for single-incision laparoscopic surgery," *IEEE Trans. Biomed. Eng.*, vol. 61, no. 9, May 2014, Art. no. 2458.

[8] H. Poon, C. Li, W. Gao, H. Ren, and C. M. Lim, "Evolution of robotic systems for transoral head and neck surgery," *Oral Oncol.*, vol. 87, pp. 82–88, 2018.

[9] J. Zhao, B. Feng, M. H. Zheng, and K. Xu, "Surgical robots for spl and notes: A review," *Minimally Invasive Therapy*, vol. 24, no. 1, pp. 8–17, 2015.

[10] C. Quaglia, G. Petroni, M. Niccolini, S. Caccavaro, and P. Dario, "Design of a compact robotic manipulator for single-port laparoscopy," *J. Mech. Des.*, vol. 136, no. 10, 2014, Art. no. 105001.

[11] H. Ren, "Computer-assisted transoral surgery with flexible robotics and navigation technologies: A review of recent progress and research challenges," *Crit. Rev. Biomed. Eng.*, vol. 41, no. 4/5, pp. 365–91, 2013.

[12] C. Li, X. Gu, X. Xiao, C. M. Lim, and H. Ren, "A robotic system with multichannel flexible parallel manipulators for single port access surgery," *IEEE Trans. Ind. Informat.*, vol. 15, no. 3, pp. 1678–1687, 2019.

[13] Y. Zhan, X. G. Duan, T. F. Cui, and D. Q. Han, "Craniotomy robot system based on human-machine parallel collaboration," in *Proc. IEEE Int. Conf. Mechatronics Automat.*, 2016, pp. 1119–1124.

[14] Y. Yan, L. Yu, C. Li, X. Gu, and H. Ren, "Ukf-based motion estimation of cable-driven forceps for robot-assisted surgical system," *IEEE Access*, vol. 8, pp. 94912–94922, 2020.

[15] Y. Hu, L. Zhang, W. Li, and G.-Z. Yang, "Design and fabrication of a 3-d printed metallic flexible joint for snake-like surgical robot," *IEEE Robot. Automat. Lett.*, vol. 4, no. 2, pp. 1557–1563, Apr. 2019.

[16] Y. Sun, S. Song, X. Liang, and H. Ren, "A miniature soft robotic manipulator based on novel fabrication methods," *IEEE Robot. Automat. Lett.*, vol. 1, no. 2, pp. 617–623, Jul. 2016.

[17] C. Li, X. Gu, X. Xiao, C. M. Lim, X. Duan, and H. Ren, "A flexible transoral robot towards covid-19 swab sampling," *Front. Robot. AI*, to be published, doi: 10.3389/frobt.2021.612167.

[18] X. Gu, C. Li, X. Xiao, C. Ming, and L. H. Ren, "A compliant transoral surgical robotic system based on a parallel flexible mechanism," *Ann. Biomed. Eng.*, vol. 47, pp. 1329–1344, 2019.

[19] Q. Liu, J. Chen, S. Shen, B. Zhang, and H. Ren, "Design, kinematics, simulation of omni-directional bending reachability for a parallel structure forceps manipulator," in *Proc. 6th IEEE Int. Conf. Biomed. Robot. Biomechatronics*, 2016, pp. 371–376.

[20] C. Li *et al.*, "A visual servo-based teleoperation robot system for closed diaphyseal fracture reduction," *Proc. Inst. Mech. Eng., Part H: J. Eng. Med.*, vol. 229, no. 9, 629–637, 2015.

[21] L. Wu, S. Song, K. Wu, C. M. Lim, and H. Ren, "Development of a compact continuum tubular robotic system for nasopharyngeal biopsy," *Med. Biol. Eng. Comput.*, vol. 55, no. 3, pp. 403–417, 2016.

[22] A. L. Orekhov, C. B. Black, J. Till, S. Chung, and D. C. Rucker, "Analysis and validation of a teleoperated surgical parallel continuum manipulator," *IEEE Robot. Automat. Lett.*, vol. 1, no. 2, pp. 828–835, Jul. 2016.

[23] T. da Veiga *et al.*, "Challenges of continuum robots in clinical context: A review," *Prog. Biomed. Eng.*, vol. 2, 2020, Art. no. 032003.

[24] N. Simaan *et al.*, "Design and integration of a telerobotic system for minimally invasive surgery of the throat," *Int. J. Robot. Res.*, vol. 28, no. 9, pp. 1134–1153, 2009.

[25] H. Abbi *et al.*, "Advances in haptics, tactile sensing, and manipulation for robot-assisted minimally invasive surgery, noninvasive surgery, and diagnosis," *J. Robot.*, vol. 2012, no. 1, p. 14, 2012.

[26] C. Li, N. K. K. King, and H. Ren, "Preliminary development of a skull-mounted lightweight parallel robot toward minimally invasive neurosurgery," in *Proc. Int. Symp. Med. Robot.*, 2018, pp. 1–6.

[27] Z. Li, L. Wu, H. Ren, and H. Yu, "Kinematic comparison of surgical tendon-driven manipulators and concentric tube manipulators," *Mechanism Mach. Theory*, vol. 107, pp. 148–165, Jan. 2017.

[28] S. S. Groothuis, S. Stramigioli, and R. Carloni, "Modeling robotic manipulators powered by variable stiffness actuators: A graph-theoretic and port-hamiltonian formalism," *IEEE Trans. Robot.*, vol. 33, no. 4, pp. 807–818, Aug. 2017.

[29] C. Li, X. Gu, X. Xiao, C. M. Lim, and H. Ren, "Flexible robot with variable stiffness in transoral surgery," *IEEE/ASME Trans. Mechatronics*, vol. 25, no. 1, pp. 1–10, Feb. 2020.

[30] N. G. Cheng *et al.*, "Design and analysis of a robust, low-cost, highly articulated manipulator enabled by jamming of granular media," in *Proc. IEEE Int. Conf. Robot. Automat.*, 2012, pp. 4328–4333.

[31] M. J. Telleria, M. Hansen, D. Campbell, A. Servi, and M. L. Culpepper, "Modeling and implementation of solder-activated joints for single-actuator, centimeter-scale robotic mechanisms," in *Proc. IEEE Int. Conf. Robot. Automat.*, May 2010, pp. 1681–1686.

[32] A. M. Okamura, "Methods for haptic feedback in teleoperated robot-assisted surgery," *Ind. Robot. Int. J.*, vol. 31, no. 6, pp. 499–508, 2004.

[33] H. M. Le, T. N. Do, and S. J. Phee, "A survey on actuators-driven surgical robots," *Sensors Actuators A. Phys.*, pp. 323–354, 2016.

[34] L. Cao *et al.*, "Sewing up the wounds: A robotic suturing system for flexible endoscopy," *IEEE Robot. Automat. Mag.*, vol. 27, no. 3, pp. 45–54, Sep. 2020.